Citrate or hydrotalcite ?

As the precursor of Pt or Ru-doped Ni/Mg(Al)O catalyst for propane oxidative reforming

Yingying Zhan,[1] Dalin Li,[1] Kazufumi Nishida,[1] Tetsuya Shishido,[2] Yasunori Oumi,[1] Tsuneji Sano[1] and Katsuomi Takehira[1]*

[1]*Department of Chemistry and Chemical Engineering, Graduate School of Engineering, Hiroshima University, Kagamiyama 1-4-1, Higashi-Hiroshima 739-8527, Japan*
[2]*Department of Molecular Engineering, Graduate School of Engineering, Kyoto University, Katsura 1, Nishikyo-ku, Kyoto 615-8510, Japan*

Received 2008

*Correspondence should be addressed to:

Professor Katsuomi Takehira
Department of Chemistry and Chemical Engineering,
Graduate School of Engineering, Hiroshima University,
Kagamiyama 1-4-1, Higashi-Hiroshima, 739-8527, Japan
Phone : (+81-824)-24-6488
Telefax: (+81-824)-24-6488
E-mail: takehira@hiroshima-u.ac.jp

Abstract

Trace amounts of Pt- and Ru-doped Ni/Mg(Al)O catalysts were prepared by a citrate method and tested in the oxidative reforming of C_3H_8 under daily start-up and shut-down (DSS) operation. The activity and the sustainability of the catalysts were compared with those of the Pt- and Ru-doped Ni/Mg(Al)O catalysts derived from hydrotalcite (HT) precursor. The DSS operation of C_3H_8 reforming was carried out with O_2 gas or O_2/H_2O mixed gas between 200 ºC and 600 or 700 ºC under air purging conditions. The catalysts underwent steaming treatment with H_2/H_2O mixed gas at 900 ºC for 10 h. This allowed us to test the effect of Ni sintering on the catalyst deactivation. Coking was significantly suppressed on both HT- and citrate-derived Ni catalysts. Although both preparations produced highly dispersed Ni particles on the catalysts, the HT-derived catalysts exhibited more finely dispersed Ni particles, resulting in higher activity values than those of the citrate-derived catalysts. The regenerative activity due to redispersion of sintered Ni particles was enhanced over the HT-derived catalysts compared with the activity over citrate-derived catalysts. Although a clear redispersion of Ni particles was not observed in the oxidative reforming, i.e., in the absence of steam, the size decrease in Ni particles was more significant over the HT-derived catalysts than over the citrate-derived catalysts. The Mg(Al)O periclase structure derived from Mg-Al HT likely plays an important role in the regenerative activity of Pt- and Ru-Ni/Mg(Al)O catalysts. Pt-doping was more effective than Ru for the catalyst sustainability in the oxidative reforming of C_3H_8.

Key Words: C_3H_8 reforming, H_2 production, Pt or Ru-Ni/Mg(Al)O catalyst, citrate, hydrotalcite.

1. Introduction

The citrate method has been frequently applied in the preparation of supported metal catalysts because it produces a homogeneous precursor, followed by the formation of stable and highly dispersed metal particles, resulting in a high and sustainable catalytic activity. We prepared Ni-containing perovskites by the citrate method, leading to the formation of well dispersed Ni particles on the catalysts and finally resulting in the sustainable activity in the oxidative reforming of CH_4 [1]. We also prepared Ni/Mg(Al)O catalysts starting from hydrotalcite (HT) precursors, which exhibited high and stable activity in steam reforming (SR) and oxidative reforming of CH_4 [2,3].

SR of CH_4 has frequently been employed as the most economical way to make H_2; most often nickel catalysts are used due to the low costs and high activity [4]. However, the endothermic SR process faces a drawback because a large energy input is needed. In the non-catalytic partial oxidation (PO), the reaction requires very high temperature [4,5]. Consequently, the catalytic oxidative reforming, i.e., PO as well as autothermal steam reforming (ATSR), has received considerable attention over the past decades. Research concerning the oxidative reforming has been focused on CH_4, as it is believed to be still a future major feedstock for the production of H_2. C_3H_8 is a hopeful candidate as an alternative resource of H_2 because it has well developed marketing

infrastructure as LPG and availability for transportation. We found that doping of trace amounts of Ru bestowed the highest and the most sustainable activity on the Ni/Mg(Al)O catalyst in the PO of C_3H_8 among the noble metals tested; self-activation and enhanced activity by reduction-oxidation treatment were observed [6,7].

In H_2 production for polymer electrolyte fuel cells (PEFCs) in domestic use, the temperature varied frequently during daily start-up and shut-down (DSS) operations. Between shut-down and start-up in the DSS operation, the catalyst bed in the reformer is purged by steam or air to enhance safety. Thus, the catalyst must be stable to tolerate multiple cycles under such unusual transient conditions without deterioration. Deactivations of Ni-loaded catalysts caused by coking, sintering, or oxidation on/of Ni have been frequently reported [8-10]. Ni can be oxidized not only by gaseous oxygen, but also even in the presence of steam [11]. A trace amount of noble metal doping on the Ni/Mg(Al)O catalysts leads not only to suppression of the Ni oxidation but also to self-regeneration of the active Ni species during the DSS SR of CH_4 [12-14].

In this research, we prepared Pt- or Ru-doped Ni/Mg(Al)O by the citrate method; their catalytic behaviors in PO and ATSR of C_3H_8 were compared with the behaviors of those derived from the HT precursors. Differences were discussed focusing on both the activity and the sustainability due to the self-regeneration of active Ni particles.

2. Experimental

2.1. Catalyst preparation

Ni loaded Mg(Al)O catalysts were prepared by citrate method and by HT method and are represented as Ni/Mg(Al)O-c and Ni/Mg(Al)O-h, respectively. The citrate method has been operated as follows: the nitrates of Ni(II) (10 mmol), Mg(II) (50 mmol) and Al(III) (20 mmol) were dissolved in distilled water and heated at 60 ºC for 2 h. Citrate monohydrate (88 mmol) was then added to the aqueous solution and the mixture was heated at 60 ºC for 1 h. After the solution was heated at 90 ºC for 2 h to decompose nitrate, the temperature was gradually increased and finally kept at 110 ºC for 5 h in order to completely evaporate any residual water. After the solution had changed to a viscous liquid, citrate was carefully decomposed by heating at 180 ºC for 3 h. Finally the mixed oxide, $Mg_{2.5}(Al,Ni_{0.5})O$-c, was obtained as powders, calcined at 850 ºC for 5 h and used as the Ni/Mg(Al)O-c catalyst precursor.

The HT method has been performed using the same amount of nitrates of Ni(II), Mg(II) and Al(III) as the citrate method following the previous works [11-14]; $Mg_{2.5}(Ni_{0.5})$-Al HT-like precursor was prepared by co-precipitation of the metal nitrates at pH = 10. When the HT was calcined at 850 ºC for 5 h, powders of $Mg_{2.5}(Al,Ni_{0.5})O$-h were obtained as the precursor of the $Ni_{0.5}/Mg_{2.5}(Al)O$-h catalyst. On both catalysts, Ni loading was determined to be 16.0 wt% by inductively coupled plasma spectroscopy (ICP) analyses.

Pt and Ru doping have been done following the method previously reported [13,14]; a 1.0 g portion of the powders of $Mg_{2.5}(Al,Ni_{0.5})O$-c or $Mg_{2.5}(Al,Ni_{0.5})O$-h was dipped in a 5 ml aqueous solution of Pt(IV) or Ru(III) nitrate for 1 h at room temperature, followed by drying in air at 100 ºC. The amount of Pt(IV) or Ru(III) nitrate corresponding to 0.10 wt% loading on the final Pt- or Ru-$Ni_{0.5}/Mg_{2.5}(Al)O$

catalyst was used. During the dipping, Mg(Ni)-Al HT was reconstituted from $Mg_{2.5}(Ni_{0.5},Al)O$-h due to "memory effect" on the surface of catalyst particles [13,14], whereas such reconstitution was weak on the $Mg_{2.5}(Al,Ni_{0.5})O$-c (vide infra). Pt and Ru were physically trapped in the layered structure of the HT during the reconstitution or adsorbed on the surface of the mixed oxide. After the samples were calcined at 850 ºC for 5 h, the precursors of the 0.10 wt% Pt- and Ru-$Ni_{0.5}/Mg_{2.5}(Al)O$ catalysts were obtained. The powders of the precursors were pressed to particles of 0.36-0.60 mm in diameter and these particles were used in the reforming reactions.

As a control, 13.5 wt% Ni/γ-Al_2O_3 catalyst was prepared by an incipient wetness method using γ-Al_2O_3 (ALO8) and an aqueous solution of Ni(II) nitrate, followed by calcination at 850 ºC for 5 h. Commercial Ni and Ru catalysts were supplied from Süd-Chemie Catalysts Japan, Inc. and were also used as controls. Both FCR (12 wt% Ni/α-Al_2O_3) and RUA (2 wt% Ru/α-Al_2O_3) catalysts as received were crushed to fine powders, pressed to particles of 0.36-0.60 mm in diameter and used in the reforming reactions.

2.2. Characterization of catalyst

The structures of the catalysts were studied by using powder X-ray diffraction (XRD), transmission electron microscopy (TEM), temperature-programmed oxidation (TPO), ICP, temperature programmed reduction (TPR), N_2 and H_2 adsorption method.

XRD was recorded on a Mac Science MX18XHF-SRA powder diffractometer with monochromatized Cu$K\alpha$ radiation (λ = 0.154 nm) at 40 kV and 30 mA. The diffraction pattern was identified through comparison with those included in the JCPDS

(Joint Committee of Powder Diffraction Standards) database. The particle size of Ni metal on the catalyst was calculated from Scherrer's equation: $d = K\lambda/\beta \cos\theta$; β, full width at half maximum; $K = 0.94$ and $\lambda = 1.5405$ Å.

TEM images were obtained on a FE-TEM Hitachi HF-2200 instrument. The samples were crushed to fine powders, dispersed in heptane using supersonic waves, and deposited on a Cu TEM grid with a holey carbon film.

TPO experiment was performed on the catalyst after the reaction from room temperature to 900 °C at a heating rate of 2.5 °C min^{-1} in a mixed gas flow of O_2/N_2 (5/20 ml min^{-1}). The amount of coke formed on the catalyst was estimated from the amount of CO_2 formed during the TPO experiment. No CO was detected during the TPO.

ICP measurement was performed with a Seiko SPS 7700. The content of each metal component was determined after the sample was completely dissolved using diluted hydrochloric acid and a small amount of hydrofluoric acid.

TPR data of the catalyst were recorded at a heating rate of 10 ºC min^{-1} using a H_2/Ar (5/95 ml min^{-1}) mixed gas as reducing gas after passing through a 13X molecular sieve trap to remove water. A U-shaped quartz tube reactor (6 mm i.d.) equipped with a TCD for monitoring the H_2 consumption was used. Prior to the TPR measurements, the sample was calcined at 300 ºC for 2 h in an O_2/Ar (10/40 ml min^{-1}) mixed gas.

The N_2 adsorption (-196 °C) study was conducted to examine the BET surface area of the samples after the calcination. The measurement was performed on a Bell-Japan Belsorpmini. The samples were pretreated in N_2 at 200 °C for 10 h before the measurements were obtained.

Ni dispersion was determined by static equilibrium adsorption of H_2 at ambient temperature using the pulse method. A 50 mg portion of the catalyst was reduced at 900 ºC in a H_2/N_2 (5/20 ml min^{-1}) mixed gas for 1 h; the reduced catalyst was used for the measurement. During the pulse experiment, the amount of H_2 was monitored by a TCD-gas chromatograph. Uptake of H_2 at monolayer coverage of the Ni species was used to estimate Ni metal dispersion and particle size. The equation used to calculate dispersion was:

$$\%D = 1.17X / Wf \quad (1)$$

where X = H_2 uptake in μmoles / g of catalyst, W = the weight percent of nickel, and f = the fraction of nickel reduced to the metal, i.e., reduction degree. The reduction degree was calculated from the amount of H_2 consumed in the TPR measurements. Average crystallite diameters d were calculated from $\%D$ assuming spherical metal crystallites [15]:

$$d = 971 / (\%D) \quad (2)$$

2.3. Kinetic measurements

Reforming of C_3H_8 was conducted in a DSS-like mode using a fixed bed-flow reactor over a 50-mg catalyst sample; PO and ATSR were carried out in $C_3H_8/O_2/N_2$ (10.0/18.7/71.3 ml min^{-1}) and $C_3H_8/H_2O/O_2/N_2$ (10.0/60.0/15.0/25.0 ml min^{-1}), respectively. The catalyst was used as particles (0.36-0.60 mm in diameter) dispersed in 50 mg of quartz beads. A U-shaped quartz reactor was used, with the catalyst bed near the bottom. The thermocouple to control the reaction temperature was placed at the center of the catalyst bed. Product gases were analyzed by online TCD-gas

chromatography. The conversions of both C_3H_8 and O_2 and the selectivity to the products were calculated using N_2 as the internal standard and the following equations:

$$C_3H_8 \text{ Conv.} = (C_3H_{8in} - C_3H_{8out})/C_3H_{8in} \times 100$$

$$O_2 \text{ Conv.} = (O_{2in} - O_{2out})/O_{2in} \times 100$$

$$H_2 \text{ Sel.} = H_{2out}/X \times 100$$

$$CO \text{ Sel.} = CO_{out}/Y \times 100$$

$$CO_2 \text{ Sel.} = CO_{2out}/Y \times 100$$

$$CH_4 \text{ Sel.} = CH_{4out}/Y \times 100$$

$$C_2H_4 \text{ Sel.} = (C_2H_{4out} \times 2)/Y \times 100$$

$$C_2H_6 \text{ Sel.} = (C_2H_{6out} \times 2)/Y \times 100$$

$$C_3H_6 \text{ Sel.} = (C_3H_{6out} \times 3)/Y \times 100$$

$$H_2O \text{ Sel.} = H_2O_{out}/X \times 100$$

where

$$X = H_{2out} + H_2O_{out} + (CH_{4out} + C_2H_{4out}) \times 2 + (C_2H_{6out} + C_3H_{6out}) \times 3$$

$$Y = CO_{out} + CO_{2out} + CH_{4out} + (C_2H_{4out} + C_2H_{6out}) \times 2 + C_3H_{6out} \times 3$$

The DSS-like operation was performed between 200 °C and 700 °C [13,14]. After the catalyst was prereduced in a H_2/N_2 (5/25 ml min^{-1}) at 900 °C for 60 min, the reaction was started at 700 °C. After 90 min of reaction at 700 °C, the reactor was cooled to 200 °C under purging by stopping C_3H_8. The reactor was held at 200 °C for 30 min, after which the temperature was again raised to 700 °C still under purging. When the temperature reached 700 °C, the reaction was again started by adding C_3H_8 into the purging gas. This reaction was carried out at 700 °C for 90 min, followed by purging. Thus the cycle reaction was repeated four times to perform the DSS-like

operation. As purging gas, O_2/N_2 (18.7/71.3 ml min^{-1}) and O_2/N_2 (15.0/25.0 ml min^{-1}) were used for PO and ATSR, respectively. If necessary, the reaction temperature was decreased to 600 ºC.

Steaming treatment of the catalyst was carried out using the fixed-bed flow reactor in $H_2/H_2O/N_2$ (20/100/25 ml min^{-1}) for 10 h at 900 °C. Each 300 mg of the catalyst was steamed, and a 50-mg catalyst sample after steaming was used for the catalytic reaction in both stationary and DSS operations of C_3H_8 reforming as described above.

3. Results and Discussion

3.1. Physicochemical properties of the catalysts.

Specific surface area and reduction degree of the catalysts before and after steaming are shown in Table 1 together with H_2 uptake and Ni dispersion on the catalysts. The surface area was large before steaming, almost the same for both $Ni_{0.5}/Mg_{2.5}$(Al)O-c and $Ni_{0.5}/Mg_{2.5}$(Al)O-h catalysts, and decreased after doping with Pt and Ru. After steaming, the surface area decreased significantly for both catalysts. The reduction degree was slightly smaller on Ni/Mg(Al)O-h than on Ni/Mg(Al)O-c, indicating that a larger part of Ni was reduced on Ni/Mg(Al)O-c than Ni/Mg(Al)O-h. The H_2 uptake was almost 1.5 times larger on Ni/Mg(Al)O-h than on Ni/Mg(Al)O-c, indicating that Ni was more finely dispersed on Ni/Mg(Al)O-h than on Ni/Mg(Al)O-c.

Metal particle sizes were calculated from the XRD and the H_2 uptake measurements (Table 2). Before steaming, Ni particles sizes were found to be smaller

on Ni/Mg(Al)O-h than on Ni/Mg(Al)O-c by both measurements. After steaming too, Ni particle sizes were also smaller on Ni/Mg(Al)O-h than on Ni/Mg(Al)O-c although a heavy sintering of Ni metal particles took place on both catalysts. The large discrepancy in Ni particle sizes observed between XRD and H_2 uptake measurements seems due to the formation of polycrystalline Ni particles, whose density was especially enhanced on the citrate-derived catalysts after steaming treatment. Judging from the higher Ni reduction degree on Ni/Mg(Al)O-c than on Ni/Mg(Al)O-h, we conclude that the latter produced more developed Mg(Al)O periclase structure than the former (vide infra), resulting in a larger amount of Ni incorporation in the Mg(Ni,Al)O solid solution in the latter catalysts. This would result in formation of smaller-sized Ni particles on Ni/Mg(Al)O-h than on Ni/Mg(Al)O-c after reduction. We conclude that Ni/Mg(Al)O-h produced more finely dispersed Ni particles after reduction than Ni/Mg(Al)O-c did.

The 13.5 wt% Ni/γ-Al_2O_3 exhibited a slightly smaller surface area, a lower H_2 uptake, a lower Ni dispersion and the highest reduction degree compared with $Ni_{0.5}/Mg_{2.5}$(Al)O-c and $Ni_{0.5}/Mg_{2.5}$(Al)O-h. Both FCR and RUA showed small surface area, very low metal dispersion and larger-sized metal particles due to the stabilization for their commercial use.

3.2. Structure of citrate- and HT-derived catalysts.

XRD patterns of $Ni_{0.5}/Mg_{2.5}$(Al)O-c, 0.1 wt% Ru-$Ni_{0.5}/Mg_{2.5}$(Al)O-c and 0.1 wt% Pt-$Ni_{0.5}/Mg_{2.5}$(Al)O-c during the preparation and after DSS PO are depicted in Fig. 1. The $Ni_{0.5}/Mg_{2.5}$(Al)O-c exhibited rather amorphous character after decomposition and periclase phase appeared after calcination at 850 ºC (Figs. 1*a* and *b*). Coq et al [16] also

prepared Ni nanoparticle/HT composites as precursors of supported Ni catalysts by citrate method. A careful control of the charge and size of the Ni-based colloids allowed them to tailor the Ni nanoparticle sizes in the final reduced samples only when Mg(Ni)-Al HT composites were prepared by the anionic exchange preparation route. However, no HT reflection was observed during the preparation of $Ni_{0.5}/Mg_{2.5}(Al)O$-c in the present work.

When $Ni_{0.5}/Mg_{2.5}(Al)O$-c after calcination was dipped in an aqueous solution of Pt(IV) or Ru(III) nitrate, weak HT reflections appeared, indicating that HT was reconstituted by a "memory effect" on the citrate-derived precursor (Figs. 1*e* and *i*). However, the reflections of HT were extremely weak compared with those observed for $Ni_{0.5}/Mg_{2.5}(Al)O$-h [6,7], indicating that less than sufficient reconstitution of HT took place on $Ni_{0.5}/Mg_{2.5}(Al)O$-c. After calcination at 850 ºC, the HT reflections disappeared and the periclase reflections were intensified (Figs. 1*f* and *j*).

In the XRD patterns of $Ni_{0.5}/Mg_{2.5}(Al)O$-c, Ni metal reflections appeared after reduction (Fig. 1c) and disappeared after DSS PO of C_3H_8 (Fig. 1*d*), suggesting that Ni oxidation took place during the reaction. The reflections of periclase were weakened after reduction, whereas they were intensified after DSS PO. This indicates that Ni^{2+} in Mg(Ni,Al)O periclase was reduced to Ni^0 and formed metallic Ni particles during reduction, whereas Ni^0 was oxidized to Ni^{2+} and was reincorporated into Mg(Ni,Al)O periclase during DSS PO. On the contrary, when 0.1 wt% Pt or Ru-$Ni_{0.5}/Mg_{2.5}(Al)O$-c was reduced, Ni metal reflections were weaker and broader than on $Ni_{0.5}/Mg_{2.5}(Al)O$-c, suggesting that Ni particles were dispersed as previously reported for the noble metal-doped $Ni_{0.5}/Mg_{2.5}(Al)O$-h [6,7]. On both 0.1 wt% Pt and Ru-doped

$Ni_{0.5}/Mg_{2.5}$(Al)O-c, Ni metal reflection remained even after DSS PO and the peaks were slightly weakened and broadened (Figs. 1*h* and *l*). Thus Ni particles on both HT and citrate-derived catalysts were slightly dispersed during DSS PO. However, it must be noticed that both 0.1 wt% Pt and Ru-doped $Ni_{0.5}/Mg_{2.5}$(Al)O-h exhibited more finely dispersed Ni particles than the citrate-derived catalysts before and after DSS PO (Table 2).

TEM images of 0.1 wt% Pt-$Ni_{0.5}/Mg_{2.5}$(Al)O-c and 0.1 wt% Pt-$Ni_{0.5}/Mg_{2.5}$(Al)O-h after steaming and DSS PO of C_3H_8 are depicted in Fig. 2. Both catalysts after steaming exhibited sintered Ni metal particles (Figs. 2a and c). No significant redispersion was observed after steaming, followed by DSS PO (Figs. 2b and d); large-sized Ni metal particles still remained even after DSS PO although the average size of Ni metal particles decreased as observed in the XRD results (Table 2). Thus no clear redispersion was observed in the present DSS PO contrarily to the previous results reported for 0.1 wt% Pt-$Ni_{0.5}/Mg_{2.5}$(Al)O-h after steaming followed by DSS SR of CH_4 [13,14]. As already shown in Table 2, heavy Ni sintering took place together with enhanced spinel formation on $Ni_{0.5}/Mg_{2.5}$(Al)O-c, 0.1 wt% Pt- and 0.1 wt% Ru-doped $Ni_{0.5}/Mg_{2.5}$(Al)O-c (Fig. 3) after steaming treatment. The sizes of sintered Ni particles on the citrate-derived catalysts were considerably larger than those on the HT-derived catalysts, i.e., $Ni_{0.5}/Mg_{2.5}$(Al)O-h, 0.1 wt% Pt- and 0.1 wt% Ru-$Ni_{0.5}/Mg_{2.5}$(Al)O-h, after steaming (Table 2). When the citrate-derived catalysts after steaming were used in the DSS PO of C_3H_8, the Ni particle sizes decreased slightly (Table 2). However, the decrease in the Ni particle size on the citrate-derived catalysts was not significant compared with that on the HT-derived catalysts. This suggests that

the regeneration of fine Ni particles was smaller on the citrate-derived catalysts than on the HT-derived catalysts (vide infra).

3.3. TPR of citrate- and HT-derived Ni catalysts.

TPR profiles of $Ni_{0.5}/Mg_{2.5}(Al)O$-c, 0.1 wt% Pt- and Ru-$Ni_{0.5}/Mg_{2.5}(Al)O$-c are depicted in Fig. 4 together with those of FCR and RUA. RUA and FCR showed the reduction peaks of Ru and Ni at 110 - 147 °C and 443 °C, respectively. The former temperature, 110 - 147 °C, coincides with 130 °C observed for 1.0 wt% Ru/CeO_2 prepared by impregnation [17] and with 125 °C observed for 1.0 wt% Ru/A_2O_3 prepared by emulsion method [18]. The latter temperature, 443 °C, is between 355 °C for pure NiO [19] and 585 °C for 10 wt% Ni/γ-Al_2O_3 [20]. Ni reduction temperature on 10 wt% Ni/γ-Al_2O_3 decreased from 585 °C to 409 °C by increasing the calcination temperature from 500 °C to 1300 °C [20]. With increase in the calcination temperature, γ-Al_2O_3 was converted to θ- and finally to α-Al_2O_3, indicating that Ni supported on α-Al_2O_3 exhibited the low reduction temperature of 445 °C due to a decrease in the metal-support interaction. This clearly indicates that Ni metal was weakly bound to the surface of α-Al_2O_3 for the FCR catalyst.

When Ni was supported on Mg(Al)O-c, the Ni reduction temperature increased to 885 °C, suggesting Ni incorporation into Mg(Al)O periclase (Fig. 4a). Ru or Pt doping caused a decrease in the Ni reduction temperature to 822 °C and 835 °C (Figs. 4d and g), respectively, probably due to easy reduction of Ru or Pt followed by hydrogen spillover from the noble metals to Ni^{2+} in the periclase or by the formation of alloy [13,14]. After steaming, the Ni reduction peak was separated into two peaks; one

appeared between 282 and 327 °C and another was observed between 910 and 939 °C. The former is ascribed to NiO separated from Mg(Ni,Al)O periclase and the latter is due to the sintering of Mg(Ni,Al)O periclase of low Ni content [13,14]. When the catalysts after steaming were applied in the DSS PO, the peak around 280 °C still remained, whereas the peak around 920 °C disappeared and a new peak appeared between 530 and 564 °C.

TPR profiles of $Ni_{0.5}/Mg_{2.5}$(Al)O-h, 0.1 wt% Pt- and Ru-$Ni_{0.5}/Mg_{2.5}$(Al)O-h are depicted in Fig. 5. The Ni reduction peaks appeared at higher temperatures on the HT-derived catalysts than on the citrate-derived catalysts: 849 °C (Fig. 5d) > 822 °C for Ru-doping and 856 °C (Fig. 5g) > 835 °C for Pt-doping, probably due to an enhanced incorporation of Ni in Mg(Al)O periclase in the former. This was also confirmed by the lower reduction degree of the HT-derived catalysts compared to the citrate-derived catalysts (Table 1). On both citrate- and HT-derived catalysts, the Ni reduction temperature decreased by Pt- and Ru-doping; moreover, the Ru-doping exhibited slightly lower reduction temperature than the Pt-doping. The profiles observed on the HT-derived catalysts (Fig. 5) were almost identical to those observed on the citrate-derived catalysts (Fig. 4) during steaming followed by DSS PO. After steaming, the Ni reduction peak was separated into two peaks: one between 149 and 334 °C and the other between 895 and 940 °C. The former is ascribed to NiO separated from Mg(Ni,Al)O periclase and the latter is ascribed to the sintered Mg(Ni,Al)O periclase of low Ni content [13,14]. When these catalysts were further followed by DSS PO, the peak at the high temperature (895 - 940 °C) disappeared and new peaks appeared between 530 and 560 °C, whereas the low temperature peaks still remained at ca.

290 °C. However the peak around 885 °C was not regenerated for both HT- and citrate-derived catalysts after steaming, followed by DSS PO. It must be noticed that this peak was regenerated after steaming followed by DSS SR, indicating the regeneration of noble metal-Ni bimetallic species on Mg(Ni,Al)O periclase [13,14]. Thus TPR results also suggest no clear regeneration of active Ni species in the present DSS PO of C_3H_8.

3.4. Activity and sustainability of citrate- and HT-derived Ni catalysts in DSS PO.

The sustainability for a long term reaction is an important property required for the reforming catalysts in the PEFCs; this seems mainly to depend on the anti-sintering property of the catalysts. The catalyst-life tests have been frequently performed by using an actual reformer for several months or years. To simulate the effect of catalyst ageing in use, researchers often used steaming for a short period [21]; this treatment was meant to simulate accelerated ageing of the catalyst under conditions representative of what the catalyst would experience during SR (i.e., high-temperatures and humid, reducing atmospheres).

The DSS PO of C_3H_8 was carried out at 700 ºC over the citrate- and HT-derived Ni catalysts either before or after steaming (Fig. 6). The HT-derived catalysts (Fig. 6A) showed higher activity than the citrate-derived catalysts (Fig. 6B). After reduction, $Ni_{0.5}/Mg_{2.5}(Al)O$-h, 0.1 wt% Pt- and Ru-$Ni_{0.5}/Mg_{2.5}(Al)O$-h exhibited 100 % C_3H_8 conversion during the DSS PO, whereas 13.5 wt% Ni/γ-Al_2O_3 as a control showed a small decrease in the conversion at the fourth step reaction (Fig. 6A). Judged from the H_2 production rate, the highest activity was obtained over 0.1 wt%

Ru-$Ni_{0.5}/Mg_{2.5}$(Al)O-h, followed by 0.1 wt% Pt-$Ni_{0.5}/Mg_{2.5}$(Al)O-h, $Ni_{0.5}/Mg_{2.5}$(Al)O-h and 13.5 wt% Ni/γ-Al_2O_3, although all catalysts were slowly deactivated. After steaming, 0.1 wt% Ru-$Ni_{0.5}/Mg_{2.5}$(Al)O-h, 0.1 wt% Pt-$Ni_{0.5}/Mg_{2.5}$(Al)O-h still exhibited 100 % C_3H_8 conversion, whereas $Ni_{0.5}/Mg_{2.5}$(Al)O-h was deactivated at the fourth step, although the deactivation was extremely small. No significant decrease was observed in H_2 production rate over the HT-derived catalysts after steaming (Fig. 6A).

On the contrary, $Ni_{0.5}/Mg_{2.5}$(Al)O-c after reduction exhibited a considerable deactivation just after the first steam purging (Fig. 6B). Although a decrease in C_3H_8 conversion was not significant, H_2 production rate decreased drastically after the first air purging. This can be explained by the fact that Ni metal was completely oxidized to Ni^{2+} and incorporated into Mg(Ni,Al)O periclase lattice after DSS PO (Fig. 1d). Products contained large amounts of C_2 hydrocarbons, suggesting that cracking of C_3H_8 took place over fresh $Ni_{0.5}/Mg_{2.5}$(Al)O-c after the first air purging (vide infra). However, very interestingly, $Ni_{0.5}/Mg_{2.5}$(Al)O-c after steaming exhibited better catalytic performances than before steaming; both C_3H_8 conversion and H_2 production rate were higher during DSS PO after steaming than before steaming (Fig. 6B). This suggests that metallic Ni still remains on the catalyst after steaming, whereas Ni was quickly oxidized on the catalyst before steaming. This was clearly supported by the XRD observation of Ni metal reflections for $Ni_{0.5}/Mg_{2.5}$(Al)O-c after steaming, followed by DSS PO (Fig. 3b). It is likely that sintered Ni metal particles were rather stabilized against oxidative incorporation into Mg(Ni,Al)O. Contrarily, Pt- or Ru-doped $Ni_{0.5}/Mg_{2.5}$(Al)O-c were rather deactivated after steaming, although $Ni_{0.5}/Mg_{2.5}$(Al)O-c was stabilized by Pt- or Ru-doping and exhibited high activity (Fig. 6B).

We previously reported that $Ni_{0.5}/Mg_{2.5}(Al)O$ catalyst derived from Mg-Ni HT exhibited high reforming activity and showed no significant formation of hot spots in the catalyst bed even when this catalyst was used in the PO of CH_4; the heat produced by combustion was quickly consumed by endothermic reforming reactions due the high reforming activity of the $Ni_{0.5}/Mg_{2.5}(Al)O$ catalyst [3]. Actually, the temperature increase observed using thermocouple at the inlet of the catalyst bed was only 9 ºC for the $Ni_{0.5}/Mg_{2.5}(Al)O$ compared to 40 ºC for 13.5 wt% $Ni/\gamma\text{-}Al_2O_3$ catalyst in the CH_4 PO carried out using horizontally placed catalyst (50 mg) bed with 18 mm in length at 800 ºC. In the present work, the catalyst bed was placed vertically with the length of ca. 10 mm. It seems difficult to measure correctly temperature distribution in the catalyst bed due to heat convection and other factors.

Distribution of products and H_2 production rate during DSS PO (200-700 ºC) of C_3H_8 over $Ni_{0.5}/Mg_{2.5}(Al)O$-c and $Ni_{0.5}/Mg_{2.5}(Al)O$-h are depicted in Fig. 7. After deactivation by the first air purging, $Ni_{0.5}/Mg_{2.5}(Al)O$-c exhibited a low rate of H_2 production as well as low selectivity to syngas formation, and the reaction was accompanied by an increase in the selectivity to C_2H_4, C_2H_6 and C_3H_6 (Fig. 7A). This indicates that a cracking of C_3H_8 was enhanced over the oxidized $Ni_{0.5}/Mg_{2.5}(Al)O$-c by steam purging. On the contrary, no significant deactivation took place over $Ni_{0.5}/Mg_{2.5}(Al)O$-h even in the absence of noble metal, although slight decreases were observed for both syngas selectivity and H_2 production rate during the reaction (Fig. 7B). Product distribution in PO of C_3H_8 calculated using the thermodynamic data base "MALT" with the C_3H_8/O_2 (10/18.75 ml min^{-1}) mixed gas is depicted in Fig. 8, where the selectivity was calculated using the equations shown in the Experimental section.

Both H_2 and CO were produced selectively, whereas the selectivity CO_2 and CH_4 decreased above 700 ºC. When the product distribution in the DSS PO of C_3H_8 (Fig. 7B) was compared with that in the thermodynamic equilibrium (Fig. 8), the actual temperature of the catalyst bed seems a little higher than 700 ºC due to exothermic PO. No alkene formation was observed over $Ni_{0.5}/Mg_{2.5}(Al)O$-h. Coke formation was not significant over $Ni_{0.5}/Mg_{2.5}(Al)O$-c, although alkenes, especially C_2H_4, were formed over the catalyst. This suggests that Mg suppressed the coking, because heavy coking was observed in the DSS PO of C_3H_8 over FCR and 13.5 wt% Ni/γ-Al_2O_3 (vide infra). C_3H_8 produced C_2 and C_3 ad-species by cracking or dehydrogenation, such species may easily polymerize to polyaromatic compounds [22]. We conclude that $Ni_{0.5}/Mg_{2.5}(Al)O$-h is more sustainable than $Ni_{0.5}/Mg_{2.5}(Al)O$-c.

3.5. Coking on citrate- and HT-derived catalysts in DSS PO.

DSS PO of C_3H_8 was carried out between 200 ºC and 600 ºC over both noble metal-doped $Ni_{0.5}/Mg_{2.5}(Al)O$-c and $Ni_{0.5}/Mg_{2.5}(Al)O$-h as well as FCR, RUA and 13.5 wt% Ni/γ-Al_2O_3 (Fig. 9). More severe catalyst deactivation was observed at 600 ºC than at 700 ºC, and both Pt- and Ru-doped $Ni_{0.5}/Mg_{2.5}(Al)O$-c (Fig. 9A) were again more severely deactivated than both Pt- and Ru-doped $Ni_{0.5}/Mg_{2.5}(Al)O$-h (Fig. 9B). Further enhanced deactivation occurred on FCR, RUA and 13.5 wt% Ni/γ-Al_2O_3, among which FCR almost stopped H_2 production after the first air purging (Fig. 9B). Steaming treatment detrimentally deactivated FCR; H_2 production was totally lost even at the first step reaction. However no significant decrease in C_3H_8 conversion was observed on FCR either after air purging or steaming. This suggests that both air purging and

steaming caused Ni oxidation, resulting in an enhanced C_3H_8 cracking activity. RUA exhibited no drastic decrease in both C_3H_8 conversion and H_2 production rate even after air purging and steaming, although both values gradually decreased during DSS PO. This suggests a high sustainability of Ru against oxidative deactivation compared with that of Ni. As observed in DSS PO at 700 ºC, $Ni_{0.5}/Mg_{2.5}(Al)O$-c after steaming exhibited higher activity than before steaming also at 600 ºC (Fig. 6B). Although $Ni_{0.5}/Mg_{2.5}(Al)O$-c was considerably deactivated by steaming, such deactivation was substantially suppressed by the doping with Pt and Ru (Fig. 9B). The Pt- and Ru-doped $Ni_{0.5}/Mg_{2.5}(Al)O$-h exhibited higher activity than the Pt- and Ru-doped $Ni_{0.5}/Mg_{2.5}(Al)O$-c. Moreover, the H_2 production rate was enhanced after the first and the second air purging over fresh $Ni_{0.5}/Mg_{2.5}(Al)O$-h (Fig. 9A) as previously reported [7]. Both deactivation suppression and enhanced H_2 production are likely due to the redispersion of Ni particles via reversible reduction-oxidation through Mg(Ni,Al)O periclase (vide infra).

TPO results of the catalysts after DSS PO between 200 ºC and 600 ºC are depicted in Fig. 10. Both citrate- and HT-derived Ni catalysts exhibited small amounts of coking; $Ni_{0.5}/Mg_{2.5}(Al)O$-c, 0.61 wt%; 0.1 wt% Ru-$Ni_{0.5}/Mg_{2.5}(Al)O$-c, 0.57 wt%; 0.1wt% Pt-$Ni_{0.5}/Mg_{2.5}(Al)O$-c, 1.01 wt%; $Ni_{0.5}/Mg_{2.5}(Al)O$-h, 1.05 wt%; 0.1 wt% Ru-$Ni_{0.5}/Mg_{2.5}(Al)O$-h, 1.66 wt% and 0.1 wt% Pt-$Ni_{0.5}/Mg_{2.5}(Al)O$-h, 1.13 wt%. RUA exhibited the smallest coking of 0.28 wt%, whereas coking amounts on FCR and 13.5 wt% Ni/γ-Al_2O_3 were far larger as 12.0 and 17.0 wt%, respectively. RUA was the most effective for suppressing coking, followed by the citrate- and then the HT-derived Ni catalysts. Ni metal catalysts can easily induce coke deposition directly from

hydrocarbons and also due to the disproportionation of CO [23]. Moreover, C_3H_8 tends to form a larger amount of coke than CH_4 in the reforming reaction [22]. The CO_2 formation during TPO significantly depended on the types of catalyst; both HT- and citrate-derived Ni catalysts showed similar patterns of CO_2 formation; CO_2 began to form at low temperature and several peaks appeared with increasing temperature. On FCR and 13.5 wt% Ni/γ-Al_2O_3, the peak of CO_2 formation appeared between 500 and 600 ºC, suggesting that graphitic carbon formed on these catalysts. Actually such graphitic carbon formed on both catalysts was clearly observed by TEM measurements (data are not shown). It has been reported that typical graphite-like coke was ignited at high temperature around 500 ºC, whereas either reactive carbonaceous deposit or chemisorbed CO present on the surface after terminating reaction ignited at temperatures below 400 ºC [24]. On both HT- and citrate-derived Ni catalysts, CO_2 formation was observed with several peaks between 100 ºC and 400 ºC in the TPO. The amount of coke was slightly higher on the HT-derived catalysts than on the citrate derived catalysts, whereas the deactivation was lower on the former than the latter.

TEM images of Pt- or Ru-doped $Ni_{0.5}/Mg_{2.5}$(Al)O-c or $Ni_{0.5}/Mg_{2.5}$(Al)O-h after steaming followed by DSS PO are depicted in Fig. 11. The formation of graphitic carbon was clearly recognized under low magnification on 0.1 wt% Pt-$Ni_{0.5}/Mg_{2.5}$(Al)O-c and 0.1 wt% Ru-$Ni_{0.5}/Mg_{2.5}$(Al)O-h both after steaming followed by DSS PO (Figs. 11a and b). This is certainly due to the formation of large-sized Ni particles after steaming. Moreover carbon-encapsulated large-sized Ni metal particles were observed under high magnification on 0.1 wt% Pt-$Ni_{0.5}/Mg_{2.5}$(Al)O-h after steaming followed by DSS PO (Figs. 11c and d). These results suggest that the

deactivation took place not only by Ni oxidation but also by Ni-covering by carbon even on the noble metal-doped catalysts after steaming. Moreover, the redispersion of the sintered Ni particles was suppressed during DSS PO due to such surface covering of Ni particles by carbon formed from C_3H_8.

3.6. Activity of citrate- and HT-derived catalysts in DSS ATSR.

One may conclude that the HT-derived Ni catalysts exhibits higher and more sustainable activity than the citrate-derived Ni catalysts in DSS PO of C_3H_8 due to both more finely dispersed Ni particles and more developed Mg(Al)O periclase structure. ATSR, i.e., reforming of C_3H_8 in the co-presence of steam and air seems to be a good option in producing H_2 for PEFCs, because there is no need for a large external heat supply. When we consider the down stream aspects of the H_2-production for PEFCs, water gas shift and then CO elimination steps follow the reforming reaction [4]. It was reported that steam condensation at low temperature heavily damaged the Cu-catalysts for CO shift reaction [25,26]. Therefore, purging conditions must be selected to avoid such wet conditions; use of dry gas such as air will be preferable as purging gas.

DSS ATSR of C_3H_8 was carried out over the citrate- and HT-derived catalysts between 200 ºC and 600 ºC under air purging conditions (Fig. 12). Both FCR and 13.5 wt% Ni/γ-Al_2O_3 exhibited a clear deactivation just after the first air purging, whereas RUA retained rather high activity, although the activity gradually decreased during DSS ATSR. Both $Ni_{0.5}/Mg_{2.5}$(Al)O-c and $Ni_{0.5}/Mg_{2.5}$(Al)O-h were also deactivated after the first air purging, whereas Pt- and Ru-doping stabilized both HT- and citrate-derived catalysts except 0.1 wt% Ru-$Ni_{0.5}/Mg_{2.5}$(Al)O-c, that was quickly deactivated after the

first air purging. 0.1 wt% Pt-$Ni_{0.5}/Mg_{2.5}$(Al)O-h was the most active, followed by 0.1 wt% Pt-$Ni_{0.5}/Mg_{2.5}$(Al)O-c and 0.1 wt% Ru-$Ni_{0.5}/Mg_{2.5}$(Al)O-h. This argues against use of Ru as noble metal-dopant in DSS ATSR, due to its weakness under oxidative conditions. We conclude that the HT-derived catalysts exhibited higher activity than the citrate-derived catalysts; 0.1 wt% Pt doping was the most effective on $Ni_{0.5}/Mg_{2.5}$(Al)O-h, resulting in the highest activity as well as the highest sustainability.

3.7. Regenerative activity of citrate- and HT-derived catalysts in DSS PO.

According to the XRD observations (Table 2), the Ni particle size was smaller on the HT-derived catalysts (5~7 nm) than on the citrate-derived catalysts (6~8 nm) before steaming. After steaming, the sizes of Ni particles increased to 16~18 nm on the HT-derived catalysts and to 17~19 nm on the citrate-derived catalysts. The noble metal-doping caused a decrease in the Ni particle sizes on both $Ni_{0.5}/Mg_{2.5}$(Al)O-c and $Ni_{0.5}/Mg_{2.5}$(Al)O-h. The Ni particle size of 13.5 wt% Ni/γ-Al_2O_3 was slightly higher than those of both $Ni_{0.5}/Mg_{2.5}$(Al)O-c and $Ni_{0.5}/Mg_{2.5}$(Al)O-h and far lower than those of both FCR and RUA. Fresh $Ni_{0.5}/Mg_{2.5}$(Al)O-c showed no Ni metal reflection due to the Ni oxidation after DSS PO, whereas fresh $Ni_{0.5}/Mg_{2.5}$(Al)O-h exhibited Ni metal reflection even after DSS PO, indicating that Ni still kept the metallic state. We conclude that the HT-derived catalysts possess more finely dispersed Ni particles, resulting in the higher activity than the citrate-derived catalysts.

When the sample after steaming was followed by DSS PO, the Ni particle sizes decreased after DSS PO both between 200 ºC and 600 ºC and between 200 ºC and 700 ºC. This is due to the regeneration of active Ni particles, i.e., redispersion of Ni particles

via reversible reduction-oxidation between Ni^0 and Ni^{2+} assisted by hydrogen spillover and Mg(Ni,Al)O periclase structure during the DSS operation [13,14]. Ni^0 was oxidatively incorporated as Ni^{2+} into Mg(Ni,Al)O periclase under steam atmosphere, whereas Ni^{2+} was reduced to form Ni^0 particles by hydrogen spiltover from Pt or PtNi alloy on the catalysts under reaction conditions. As shown in TPR results (Figs. 4 and 5), no clear regeneration of the Mg(Ni,Al)O periclase peak at 885 °C was observed on either citrate- or HT-derived Ni/Mg(Al)O catalysts in the present work. Contrarily, the peak ascribed to Mg(Ni,Al)O periclase was clearly regenerated at 885 °C in TPR of the noble metal-doped catalysts after steaming followed by DSS SR [13,14]. This strongly suggests that steam assists the regeneration of Mg(Ni,Al)O periclase during the DSS operation; steam hydrolyzes surface MgO into $Mg(OH)_2$ and simultaneously oxidatively hydrolyzes Ni^0 into $Ni(OH)_2$, leading to the reconsitution of Mg(Ni)-Al HT and finally to the formation of Mg(Ni,Al)O periclase. When steam was replaced by oxygen in the present work, Mg(Ni,Al)O periclase regeneration was not observed clearly in TPR. However, the periclase phase was confirmed by XRD observation. Moreover, steam can be formed by the reaction between O_2 and H_2 and such steam may assist the regeneration of Mg(Ni,Al)O periclase, although its amount was too small to be detected by TPR.

Decrease in the Ni particle size was observed also on $Ni_{0.5}/Mg_{2.5}$(Al)O-c and $Ni_{0.5}/Mg_{2.5}$(Al)O-h, suggesting that regenerative activity worked, although very slowly, even in the absence of noble metal. Moreover, such decrease in the Ni particle sizes was more significant on the HT-derived catalysts than on the citrate-derived catalysts (Table 2). This is because Mg(Al)O periclase structure plays an important role in the

regenerative activity; Mg(Al)O periclase worked as an effective Ni reservoir as well as Ni disperser for supplying the active Ni particles on the catalyst surface. It is likely that the HT-derived Ni catalysts with more developed Mg(Al)O periclase structure were more active as well as more sustainable than the citrate-derived Ni catalysts.

4. Conclusion

The citrate- and the HT derived Ni/Mg(Al)O catalysts doped with trace amount of Pt- and Ru were prepared and comparatively tested in the oxidative reforming of C_3H_8 under DSS operation. The oxidative C_3H_8 reforming was carried out with O_2 gas and O_2/H_2O mixed gas between 200 ºC and 600 or 700 ºC under O_2 and the mixed gas purging conditions, respectively. Coking was significantly suppressed on both HT- and citrate-derived Ni catalysts. Although both preparations produced highly dispersed Ni particles on the catalysts, the HT-derived Ni catalysts formed more finely dispersed Ni particles, resulting in the higher activity than the citrate-derived Ni catalysts. Although the redispersion of Ni particles was not significant in the DSS PO in the absence of steam, even sintered Ni particles after steaming were more effectively redispersed, resulting in the more effective regeneration of the activity on the HT-derived catalysts than the citrate-derived catalysts. It is likely that both steam and Mg(Al)O periclase play important roles in the regenerative activity of Pt- and Ru-doped Ni/Mg(Al)O catalysts. Pt-doping on Ni/Mg(Al)O-h was the most effective for the activity and the sustainability of catalyst in the oxidative reforming of propane.

References

[1] K. Takehira, T. Shishido, M. Kondo, J. Catal. 207 (2002) 307-316.

[2] K. Takehira, T. Shishido, P. Wang, T. Kosaka, K. Takaki, Phys. Chem. Chem. Phys. 5 (2003) 3801-3810.

[3] K. Takehira, T. Shishido, P. Wang, T. Kosaka, K. Takaki, J. Catal. 221 (2004) 43-54.

[4] J.R. Rostrup-Nielsen, Catal. Today 71 (2002) 243-247.

[5] J.N. Armor, Appl. Catal. A: Gen. 176 (1999) 159-176.

[6] M. Shiraga, D. Li, I. Atake, T. Shishido, Y. Oumi, T. Sano, K. Takehira, Appl. Catal. A: Gen. 318 (2007) 143-154.

[7] D. Li, M. Shiraga, I. Atake, T. Shishido, Y. Oumi, T. Sano, K. Takehira, Appl. Catal. A: Gen. 321 (2007) 155-164.

[8] V.A. Tsipouriari, Z. Zhang, X.E. Verykios, J. Catal. 179 (1998) 283-291.

[9] H.S. Bengaard, J.K. Nørskov, J. Sehested, B.S. Clausen, L.P. Nielsen, A.M. Molenbroek, J.R. Rostrup-Nielsen, J. Catal. 209 (2002) 365-384.

[10] S. Natesakhawat, R.B. Watson, X. Wang, U.S. Ozkan, J. Catal. 234 (2005) 496-508.

[11] T. Miyata, D. Li, M. Shiraga, T. Shishido, Y. Oumi, T. Sano, K. Takehira, Appl. Catal. A: Gen. 310 (2006) 97-104.

[12] T. Miyata, M. Shiraga, D. Li, I. Atake, T. Shishido, Y. Oumi, T. Sano, K. Takehira, Catal. Commun. 8 (2007) 447-451.

[13] D. Li, I. Atake, T. Shishido, Y. Oumi, T. Sano, K. Takehira, J. Catal. 250 (2007) 299-312.

[14] D. Li, K. Nishida, Y. Zhan, T. Shishido, Y. Oumi, T. Sano, K. Takehira, Appl. Catal. A: Gen. 350 (2008) 225-236.

[15] C.H. Bartholomew, R.B. Pannell, J.L. Butler, J. Catal. 65 (1980) 335-347.

[16] C. Gérardin, D. Kostadinova, N. Sanson, D. Francova, N. Tanchoux, D. Tichit, B. Coq, Stud. Surf. Sci. Catal. 156 (2005) 357-362.

[17] T. Mitsui, K. Tsutsui, T. Matsui, R. Kikuchi, K. Eguchi, Appl. Catal. B: Env. 81 (2008) 56-63.

[18] R. Lanza, P. Canu, S.G. Järås, Appl. Catal. A: Gen. 337 (2008) 10-18.

[19] M. de los A. Cangiano, A.C. Carreras, M.W. Ojeda, M. del C. Ruiz, J. Alloy and Compounds 458 (2008) 405-409.

[20] K.V.R. Chary, P.V.T. Rao, V.V. Rao, Catal. Commun. 9 (2008) 886-893.

[21] M. Ferrandon, T. Krause, Appl. Catal. A: Gen. 311 (2006) 135-145.

[22] T. Sperle, D. Chen, R. Lødeng, A. Holmen, Appl. Catal. A: Gen. 282 (2005) 195-204.

[23] A. Valentini, N. Lenin, V. Carreño, L.F.D. Probst, P.N. Lisboa-Filho, W.H. Schreiner, E.R. Leite, E. Longo, Appl. Catal. A: Gen. 255 (2003) 211-220.

[24] M.C.J. Bradford, M.A. Vannice, Appl. Catal. A: Gen. 142 (1996) 73-96.1996.

[25] O. Ilinich, W. Ruettinger, X.-S. Liu, R. Farrauto, J. Catal. 247 (2007) 112-118.

[26] K. Nishida, I. Atake, D. Li, T. Shishido, Y. Oumi, T. Sano, K. Takehira, Appl. Catal. A: Gen. 337 (2008) 48-57.

Table 1. Physicochemical properties of the Ni and Ru catalysts before and after steaming[a]

Catalyst	BET surface area[b] (m^2 g_{cat}^{-1})		Reduction degree[c] (%)	H_2 uptake[d] (μmol g_{cat}^{-1})		Dispersion[e] (%)	
	Before	After	Before	Before	After	Before	After
$Ni_{0.5}/Mg_{2.5}(Al)O$-c	171.1	19.1	92.1	86.1	24.5	6.8	2.0
0.10 wt% Ru-$Ni_{0.5}/Mg_{2.5}(Al)O$-c	144.9	23.7	92.8	126.1	27.9	9.9	2.2
0.10 wt% Pt-$Ni_{0.5}/Mg_{2.5}(Al)O$-c	116.4	18.4	91.2	134.3	23.6	10.8	1.9
$Ni_{0.5}/Mg_{2.5}(Al)O$-h	173.6	56.8	80.7	120.7	40.2	13.1	4.4
0.10 wt% Ru-$Ni_{0.5}/Mg_{2.5}(Al)O$-h	128.7	56.4	80.0	221.9	58.4	24.0	6.3
0.10 wt% Pt-$Ni_{0.5}/Mg_{2.5}(Al)O$-h	141.2	56.9	82.5	225.3	44.3	20.6	4.0
13.5 wt% Ni/γ-Al_2O_3	106.8	61.0	100	74.4	19.3	8.1	2.1
FCR(12 wt% Ni/α-Al_2O_3)	12.3	11.7	-	0.08	-	0.0	-
RUA(2 wt% Ru/α-Al_2O_3)	11.4	10.6	-	0.18	-	0.1	-

a Steaming was carried out at 900 °C for 10 h in a mixed gas flow of $H_2/H_2O/N_2$ (20/100/25 ml min^{-1}).

b The catalysts were calcined at 850 °C for 5 h before catalytic tests.

c Calculated from the amount of H_2 consumed in the TPR measurement

d Determined by the H_2 pulse method.

e Calculated from the H_2 uptake and the reduction degree using the equation

$$\%D = 1.17X/Wf$$

where X is H_2 uptake in μmol g^{-1} of catalyst, W is the weight percent of nickel, and f is the reduction degree..

Table 2. Metal particle size of the Ni and Ru catalysts before and after steaming, and further followed by DSS PO[a]

Catalyst	Metal particle size (nm)							
	XRD[b]						H_2 uptake[c]	
	Before			After			Before	After
		After DSS PO[d]	After DSS PO[e]		After DSS PO[d]	After DSS PO[e]		
$Ni_{0.5}/Mg_{2.5}(Al)O$-c	8.2	n.d.	n.d.	18.3	17.6	17.1	14.2	49.9
0.10 wt% Ru-$Ni_{0.5}/Mg_{2.5}(Al)O$-c	6.0	5.7	5.0	19.3	16.5	16.0	9.8	44.3
0.10 wt% Pt-$Ni_{0.5}/Mg_{2.5}(Al)O$-c	6.1	5.6	8.4	17.1	15.7	14.4	9.0	51.2
$Ni_{0.5}/Mg_{2.5}(Al)O$-h	6.8	8.3	6.6	18.4	15.0	15.2	7.4	22.3
0.10 wt% Ru-$Ni_{0.5}/Mg_{2.5}(Al)O$-h	5.2	5.2	5.0	16.8	13.3	11.1	4.0	15.3
0.10 wt% Pt-$Ni_{0.5}/Mg_{2.5}(Al)O$-h	5.5	5.8	5.5	16.5	12.9	13.5	4.7	24.0
13.5 wt% Ni/γ-Al_2O_3	9.0	9.3	9.3	21.0	17.8	19.5	12.0	46.4
FCR(12 wt% Ni/α-Al_2O_3)	23.1		29.6	24.1		n.d.	-	-
RUA(2 wt% Ru/α-Al_2O_3)	(23.6)		(31.7)	(25.6)		(29.8)	-	-

a Steaming was carried out at 900 °C for 10 h in a mixed gas flow of $H_2/H_2O/N_2$ (20/100/25 ml min^{-1}).

b Calculated from the full width at half maximum of the reflections of Ni (200) plane in the XRD using the Scherrer equation.

c Calculated using the equation: d = 971/(%D)/10 where D is the dispersion [15].

d&e Each DSS (4 times SS) propane reforming was carried out under the following conditions: (d) 200-700 °C, air purge; (e) 200-600 °C, air purge.

Figure captions

Fig. 1. XRD patterns of the $Ni_{0.5}/Mg_{2.5}(Al)O$-c catalysts during preparation and after DSS PO.

(a) $Ni_{0.5}/Mg_{2.5}(Al)O$-c after decomposition; (b) $Ni_{0.5}/Mg_{2.5}(Al)O$-c after calcination; (c) $Ni_{0.5}/Mg_{2.5}(Al)O$-c after reduction; (d) $Ni_{0.5}/Mg_{2.5}(Al)O$-c after DSS PO; (e) 0.1 wt% Ru-$Ni_{0.5}/Mg_{2.5}(Al)O$-c after dipping; (f) 0.1 wt% Ru-$Ni_{0.5}/Mg_{2.5}(Al)O$-c after calcination; (g) 0.1 wt% Ru-$Ni_{0.5}/Mg_{2.5}(Al)O$-c after reduction; (h) 0.1 wt% Ru-$Ni_{0.5}/Mg_{2.5}(Al)O$-c after DSS PO; (i) 0.1 wt% Pt-$Ni_{0.5}/Mg_{2.5}(Al)O$-c after dipping; (j) 0.1 wt% Pt-$Ni_{0.5}/Mg_{2.5}(Al)O$-c after calcination; (k) 0.1 wt% Pt-$Ni_{0.5}/Mg_{2.5}(Al)O$-c after reduction; (l) 0.1 wt% Pt-$Ni_{0.5}/Mg_{2.5}(Al)O$-c after DSS PO.

(○) Mg-Al HT; (■) Mg(Al)O periclase; (▲) $MgAl_2O_4$ spinel; (●) Ni metal.

Fig. 2 TEM images of 0.1 wt% Pt-$Ni_{0.5}/Mg_{2.5}(Al)O$-h and 0.1 wt% Pt-$Ni_{0.5}/Mg_{2.5}(Al)O$-c catalysts after steaming followed by DSS PO.

a) 0.1 wt% Pt-$Ni_{0.5}/Mg_{2.5}(Al)O$-c after steaming; b) 0.1 wt% Pt-$Ni_{0.5}/Mg_{2.5}(Al)O$-c after steaming followed by DSS PO; c) 0.1 wt% Pt-$Ni_{0.5}/Mg_{2.5}(Al)O$-h after steaming; d) 0.1 wt% Pt-$Ni_{0.5}/Mg_{2.5}(Al)O$-h after steaming followed by DSS PO.

Fig. 3 XRD patterns of the $Ni_{0.5}/Mg_{2.5}(Al)O$-c catalysts after steaming followed by DSS PO.

(a) $Ni_{0.5}/Mg_{2.5}(Al)O$-c after steaming; (b) $Ni_{0.5}/Mg_{2.5}(Al)O$-c after steaming flowed by DSS PO; (c) 0.1 wt% Ru-$Ni_{0.5}/Mg_{2.5}(Al)O$-c after steaming; (d) 0.1

wt% Ru-$Ni_{0.5}/Mg_{2.5}$(Al)O-c after steaming followed by DSS PO; (e) 0.1 wt% Pt-$Ni_{0.5}/Mg_{2.5}$(Al)O-c after steaming; (f) 0.1 wt% Pt-$Ni_{0.5}/Mg_{2.5}$(Al)O-c after steaming followed by DSS PO.

(■) Mg(Al)O periclase; (▲) $MgAl_2O_4$ spinel; (●) Ni metal.

Fig. 4 TPR profiles of the $Ni_{0.5}/Mg_{2.5}$(Al)O-c catalysts.

(a) $Ni_{0.5}/Mg_{2.5}$(Al)O-c after reduction; (b) $Ni_{0.5}/Mg_{2.5}$(Al)O-c after steaming; (c) $Ni_{0.5}/Mg_{2.5}$(Al)O-c after steaming, followed by DSS PO; (d) 0.10 wt% Ru-$Ni_{0.5}/Mg_{2.5}$(Al)O-c after reduction; (e) 0.10 wt% Ru-$Ni_{0.5}/Mg_{2.5}$(Al)O-c after steaming; (f) 0.10 wt% Ru-$Ni_{0.5}/Mg_{2.5}$(Al)O-c after steaming, followed by DSS PO; (g) 0.10 wt% Pt-$Ni_{0.5}/Mg_{2.5}$(Al)O-c after reduction; (h) 0.10 wt% Pt-$Ni_{0.5}/Mg_{2.5}$(Al)O-c after steaming; (i) 0.10 wt% Pt-$Ni_{0.5}/Mg_{2.5}$(Al)O-c after steaming, followed by DSS PO; (j) FCR; (k) RUA.

Fig. 5 TPR profiles of the $Ni_{0.5}/Mg_{2.5}$(Al)O-h catalysts.

(a) $Ni_{0.5}/Mg_{2.5}$(Al)O-h after reduction; (b) $Ni_{0.5}/Mg_{2.5}$(Al)O-h after steaming; (c) $Ni_{0.5}/Mg_{2.5}$(Al)O-h after steaming, followed by DSS PO; (d) 0.10 wt% Ru-$Ni_{0.5}/Mg_{2.5}$(Al)O-h after reduction; (e) 0.10 wt% Ru-$Ni_{0.5}/Mg_{2.5}$(Al)O-h after steaming; (f) 0.10 wt% Ru-$Ni_{0.5}/Mg_{2.5}$(Al)O-h after steaming, followed by DSS PO; (g) 0.10 wt% Pt-$Ni_{0.5}/Mg_{2.5}$(Al)O-h after reduction; (h) 0.10 wt% Pt-$Ni_{0.5}/Mg_{2.5}$(Al)O-h after steaming; (i) 0.10 wt% Pt-$Ni_{0.5}/Mg_{2.5}$(Al)O-h after steaming, followed by DSS PO.

Fig. 6. C_3H_8 conversion and H_2 production rate during DSS PO of C_3H_8 between 200 and 700 °C over $Ni_{0.5}/Mg_{2.5}$(Al)O-h, $Ni_{0.5}/Mg_{2.5}$(Al)O-c and other catalysts before and after steaming.

Full line: before steaming; dotted line: after steaming.

(●) $Ni_{0.5}/Mg_{2.5}(Al)O$-h; (■) 0.10 wt% Ru-$Ni_{0.5}/Mg_{2.5}(Al)O$-h; (▲) 0.10 wt% Pt-$Ni_{0.5}/Mg_{2.5}(Al)O$-h; (×) 13.5 wt% Ni/γ-Al_2O_3; (○) $Ni_{0.5}/Mg_{2.5}(Al)O$-c; (□) 0.10 wt% Ru-$Ni_{0.5}/Mg_{2.5}(Al)O$-c; (△) 0.10 wt% Pt-$Ni_{0.5}/Mg_{2.5}(Al)O$-c.

Fig. 7 Product distributions and H_2 production rate during DSS PO of C_3H_8 between 200 and 700 °C over $Ni_{0.5}/Mg_{2.5}(Al)O$-c (A) and $Ni_{0.5}/Mg_{2.5}(Al)O$-h (B) catalysts.

Full line: conversion: (○) C_3H_8; selectivity: (●) H_2; (■) CO;(▲) CO_2; (∗) CH_4; (×) C_2H_4; (+) C_2H_6; (—) C_3H_6.

Dotted line: (●) H_2 production rate.

Fig. 8 Product selectivity in PO of C_3H_8 calculated by the thermodynamic data base "MALT" with the C_3H_8/O_2 (10/18.75 ml min^{-1}) mixed gas.

(●) H_2; (■) CO; (▲) CO_2; (◇) H_2O; (∗) CH_4.

Fig. 9 C_3H_8 conversion and H_2 production rate during DSS PO of C_3H_8 between 200 and 600 °C over $Ni_{0.5}/Mg_{2.5}(Al)O$-h, $Ni_{0.5}/Mg_{2.5}(Al)O$-c and other catalysts before and after steaming.

Full line: before steaming; dotted line: after steaming.

(●) $Ni_{0.5}/Mg_{2.5}(Al)O$-h; (■) 0.10 wt% Ru-$Ni_{0.5}/Mg_{2.5}(Al)O$-h; (▲) 0.10 wt% Pt-$Ni_{0.5}/Mg_{2.5}(Al)O$-h; (×) 13.5 wt% Ni/γ-Al_2O_3; (+) FCR; (—) RUA; (○) $Ni_{0.5}/Mg_{2.5}(Al)O$-c; (□) 0.10 wt% Ru-$Ni_{0.5}/Mg_{2.5}(Al)O$-c; (△) 0.10 wt% Pt-$Ni_{0.5}/Mg_{2.5}(Al)O$-c

Fig. 10 TPO of the catalysts after DSS PO of C_3H_8 between 200 and 600 °C.

(a) $Ni_{0.5}/Mg_{2.5}(Al)O$-c; (b) 0.10 wt% Ru-$Ni_{0.5}/Mg_{2.5}(Al)O$-c; (c) 0.10 wt%

Pt-$Ni_{0.5}/Mg_{2.5}$(Al)O-c; (d) $Ni_{0.5}/Mg_{2.5}$(Al)O-h; (e) 0.10 wt% Ru-$Ni_{0.5}/Mg_{2.5}$(Al)O-h; (f) 0.10 wt% Pt-$Ni_{0.5}/Mg_{2.5}$(Al)O-h; (g) RUA; (h) FCR; (i) 13.5 wt% Ni/γ-Al_2O_3.

Fig. 11 TEM images of 0.1 wt% Pt-$Ni_{0.5}/Mg_{2.5}$(Al)O-c, 0.1 wt% Pt-$Ni_{0.5}/Mg_{2.5}$(Al)O-h and 0.1 wt% Ru-$Ni_{0.5}/Mg_{2.5}$(Al)O-h catalysts after steaming followed by DSS PO.

a) 0.1 wt% Pt-$Ni_{0.5}/Mg_{2.5}$(Al)O-c after steaming followed by DSS PO; b) 0.1 wt% Ru-$Ni_{0.5}/Mg_{2.5}$(Al)O-h after steaming followed by DSS PO; c) 0.1 wt% Pt-$Ni_{0.5}/Mg_{2.5}$(Al)O-h after steaming followed by DSS PO; d) 0.1 wt% Pt-$Ni_{0.5}/Mg_{2.5}$(Al)O-h after steaming followed by DSS PO.

Fig. 12 C_3H_8 conversion and H_2 production rate during DSS ATSR of C_3H_8 between 200 and 600 °C over $Ni_{0.5}/Mg_{2.5}$(Al)O-h, $Ni_{0.5}/Mg_{2.5}$(Al)O-c and other catalysts.

Full line: C_3H_8 conversion; dotted line: H_2 production rate.

(●) $Ni_{0.5}/Mg_{2.5}$(Al)O-h; (■) 0.10 wt% Ru-$Ni_{0.5}/Mg_{2.5}$(Al)O-h; (▲) 0.10 wt% Pt-$Ni_{0.5}/Mg_{2.5}$(Al)O-h; (×) 13.5 wt% Ni/γ-Al_2O_3; (+) FCR; (—) RUA; (○) $Ni_{0.5}/Mg_{2.5}$(Al)O-c; (□) 0.10 wt% Ru-$Ni_{0.5}/Mg_{2.5}$(Al)O-c; (△) 0.10 wt% Pt-$Ni_{0.5}/Mg_{2.5}$(Al)O-c.

Figure 1. K. Takehira et al.

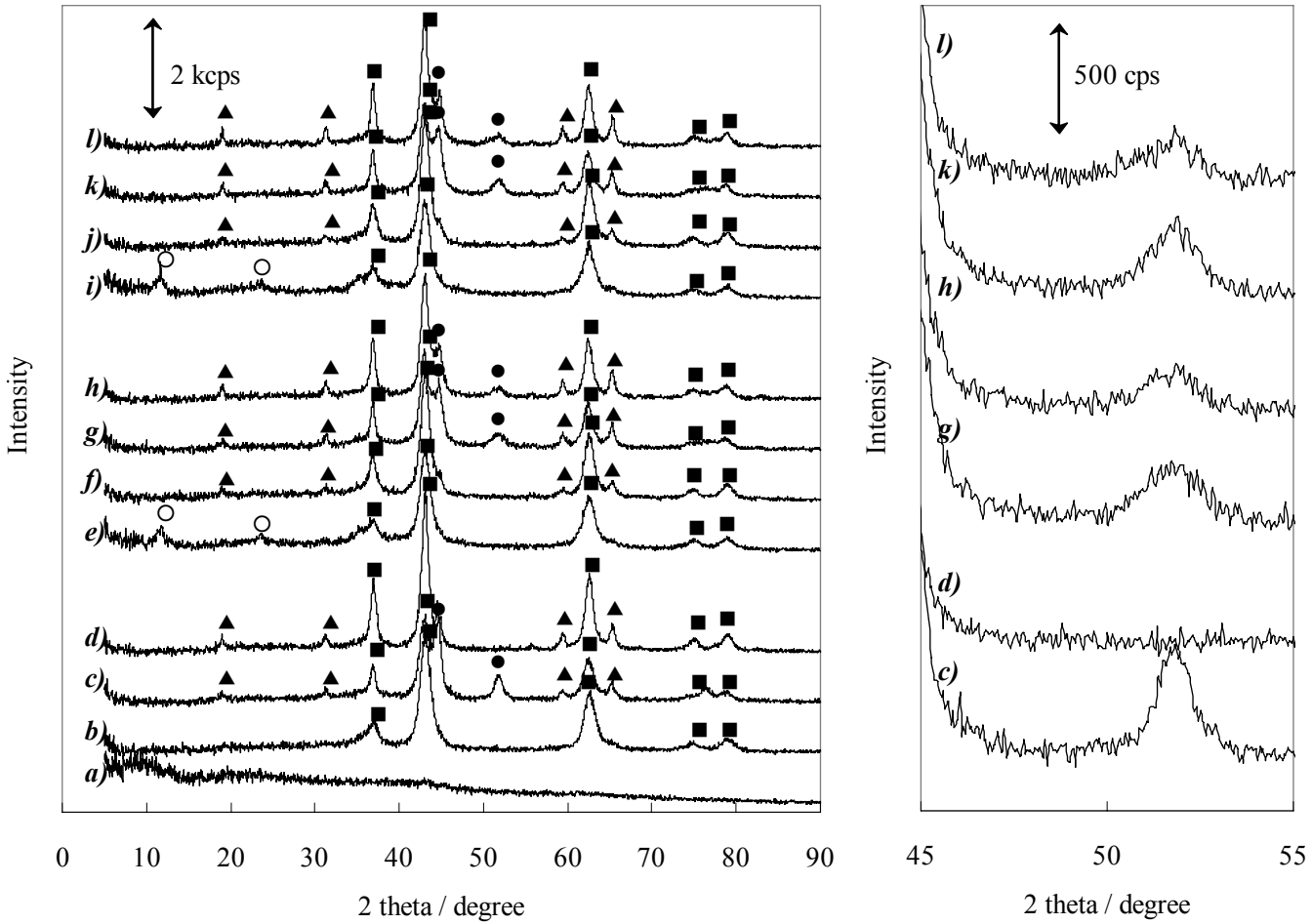

Figure 2.　K. Takehira et al.

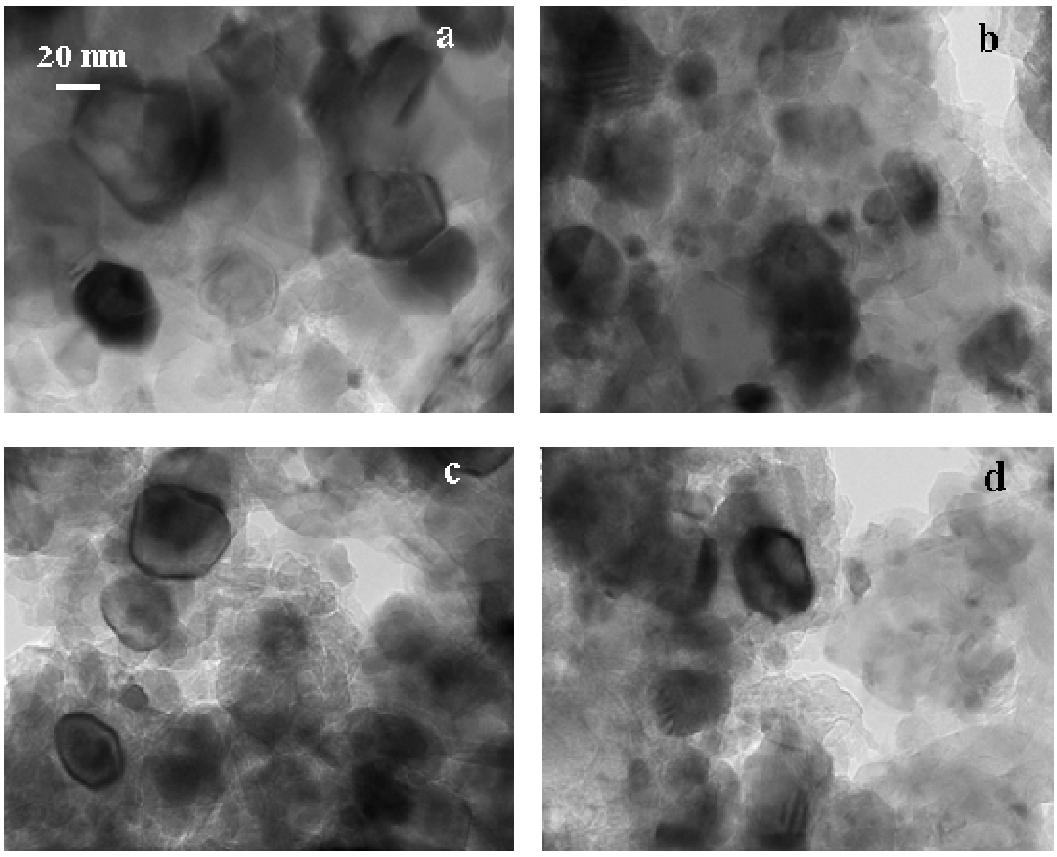

Figure 3. K. Takehira et al.

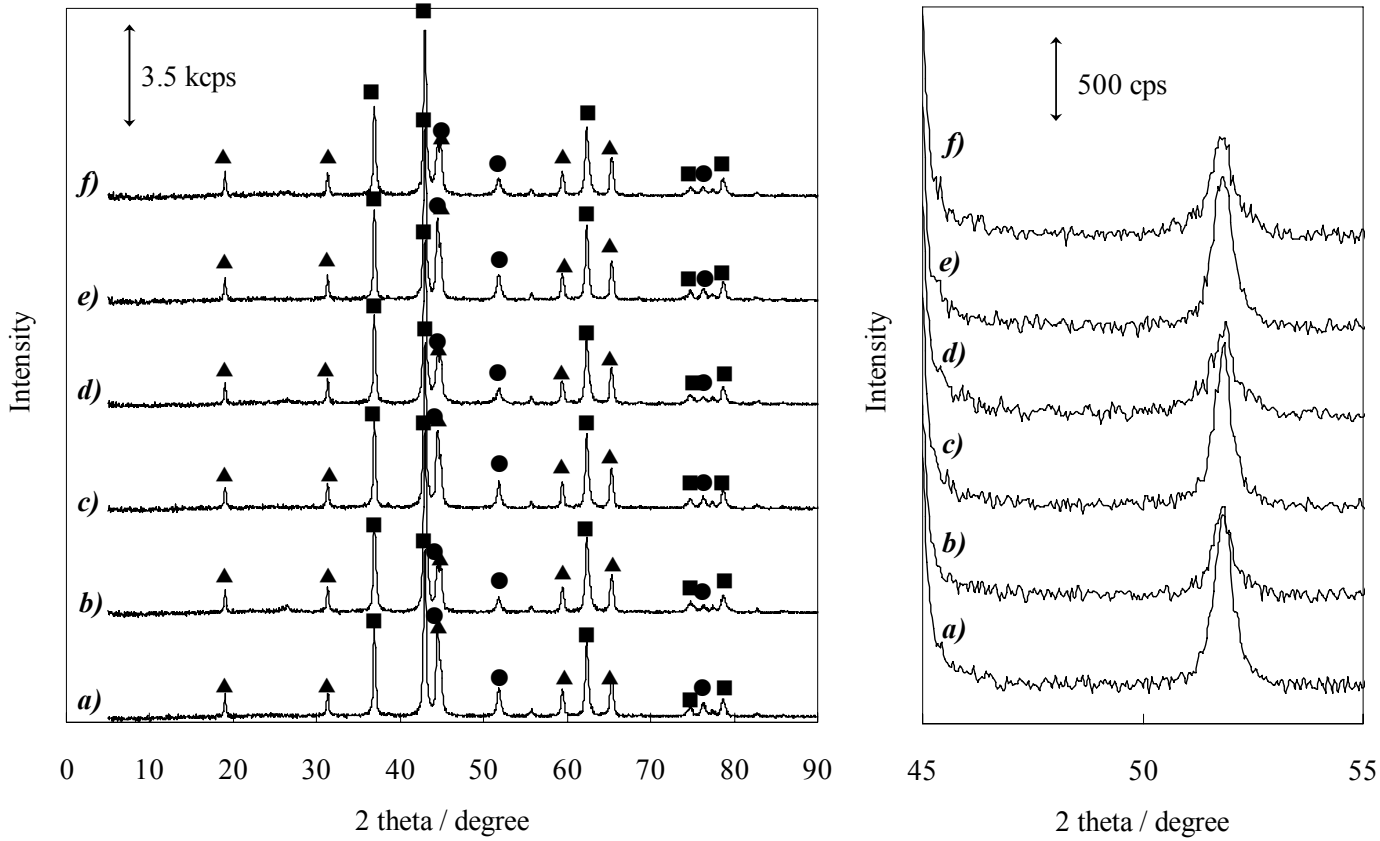

Figure 4. K. Takehira et al.

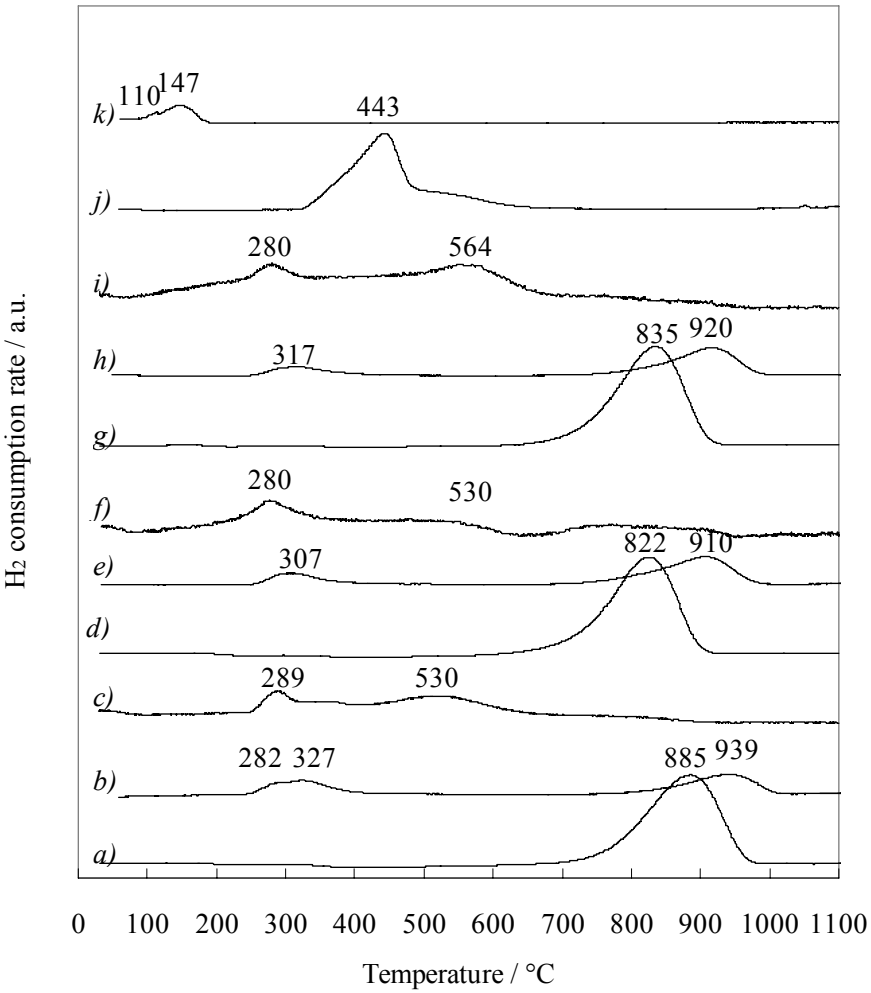

Figure 5. K. Takehira et al.

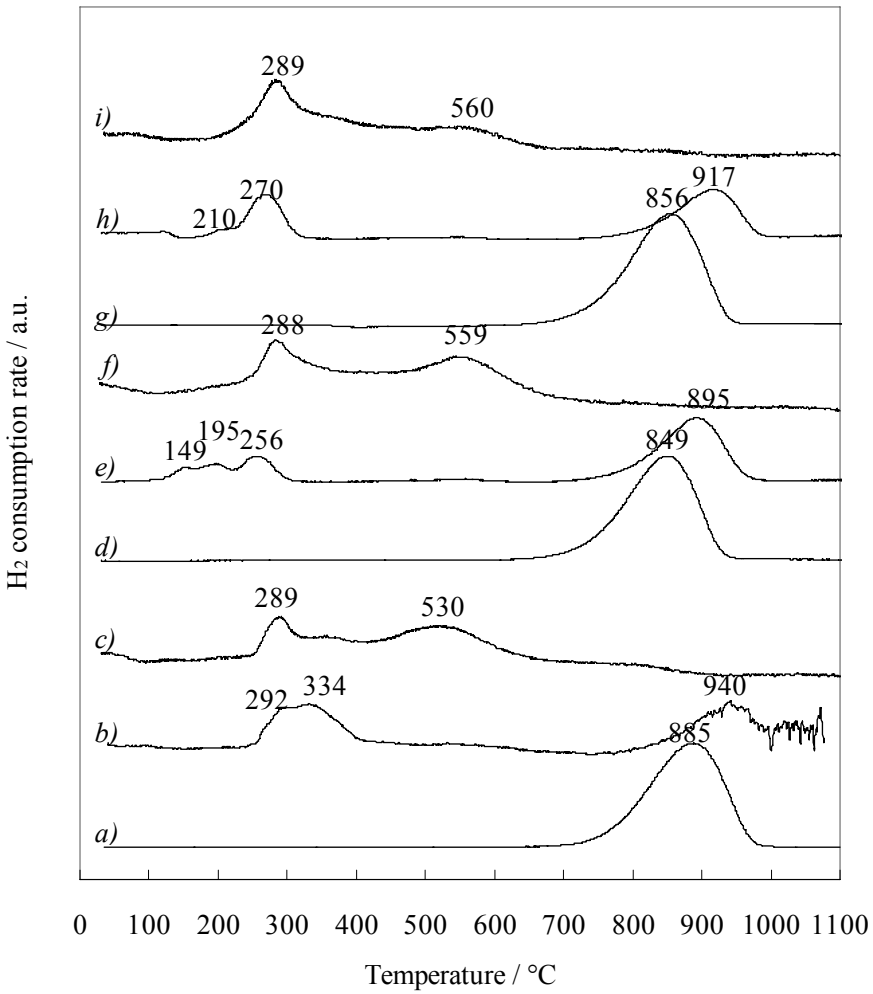

Figure 6. K. Takehira et al.

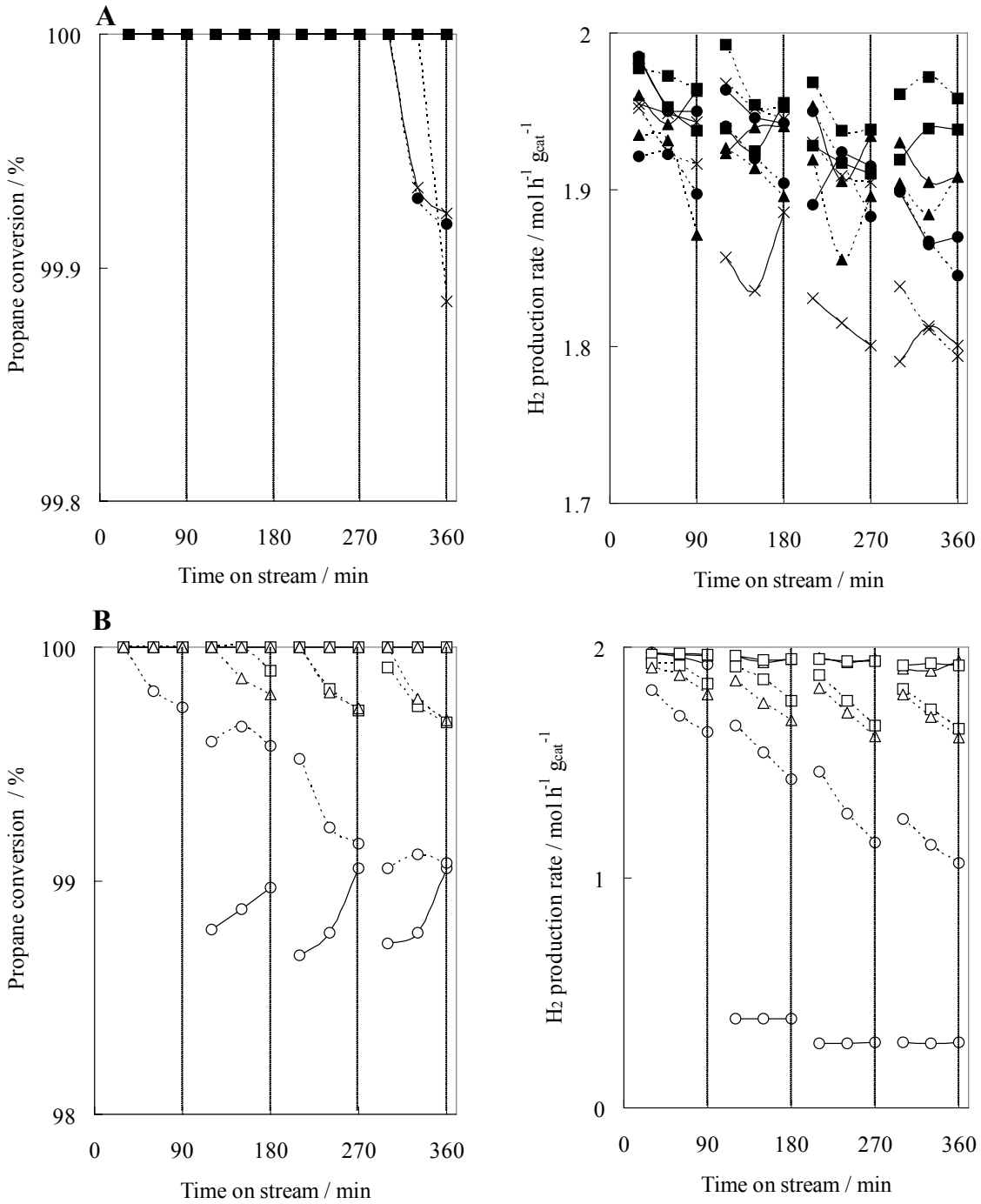

Figure 7. K. Takehira et al.

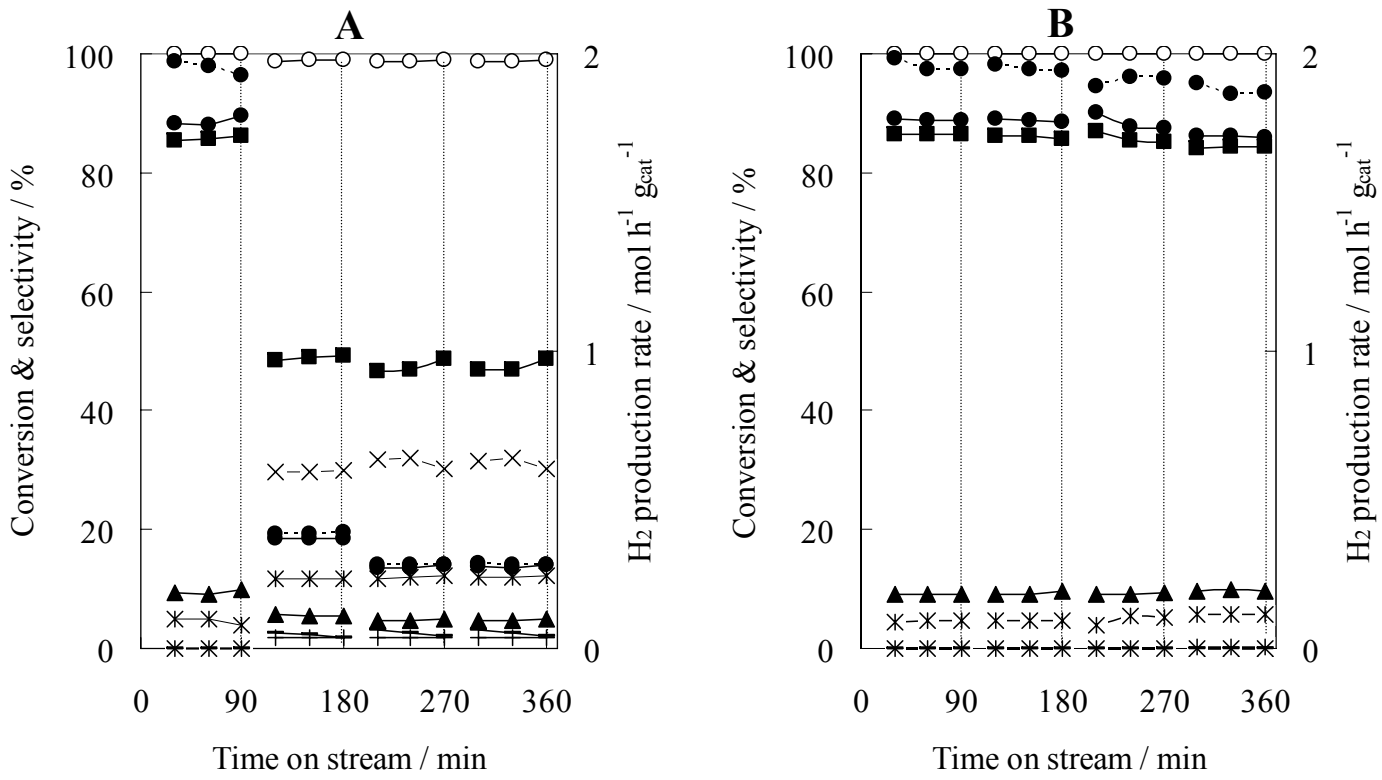

Figure 8. K. Takehira et al.

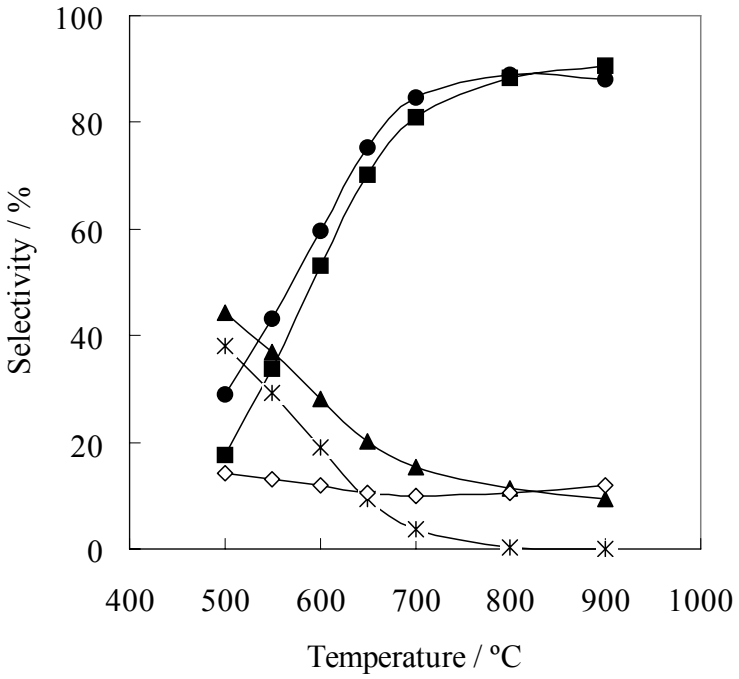

Figure 9. K. Takehira et al.

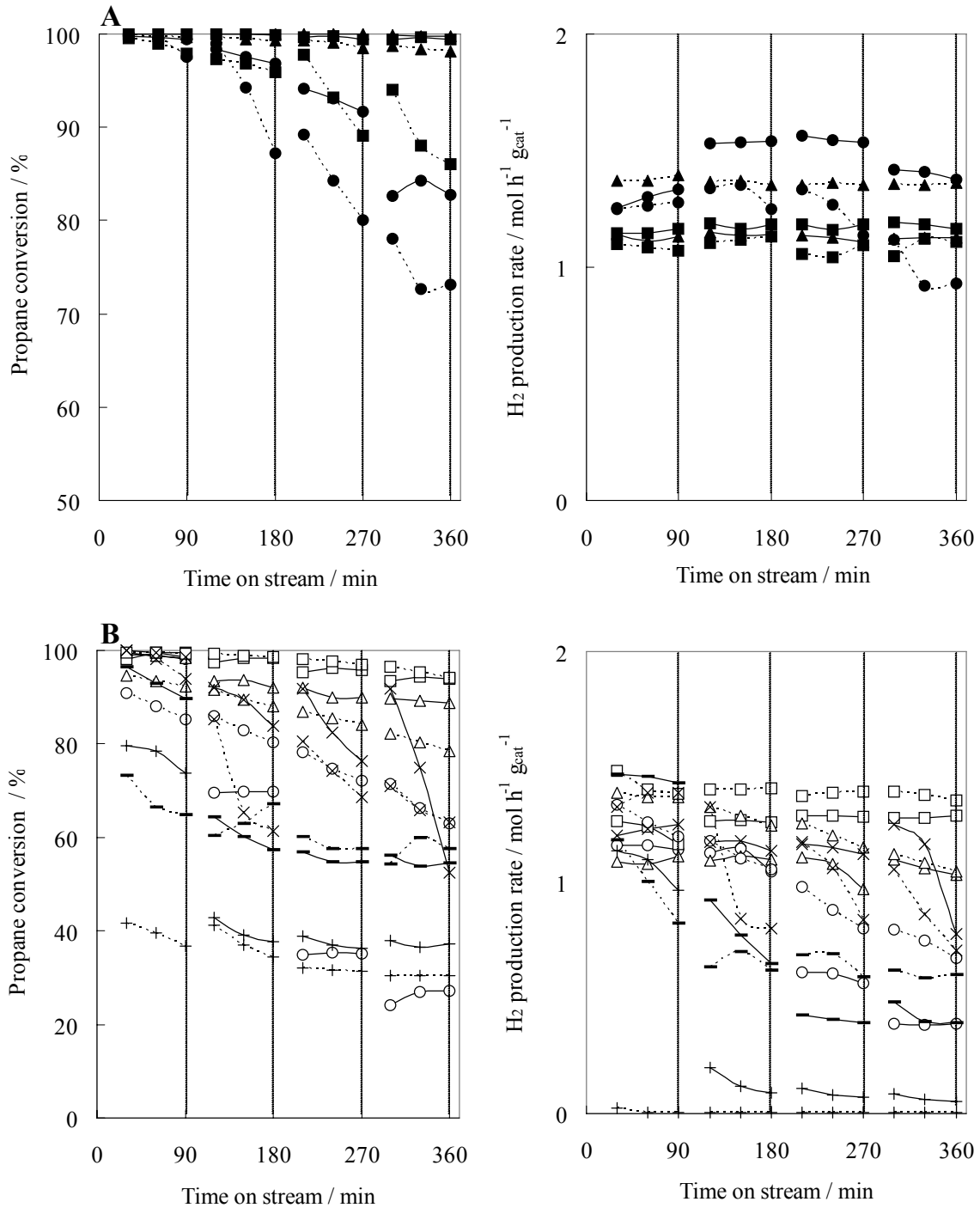

Figure 10. K. Takehira et al.

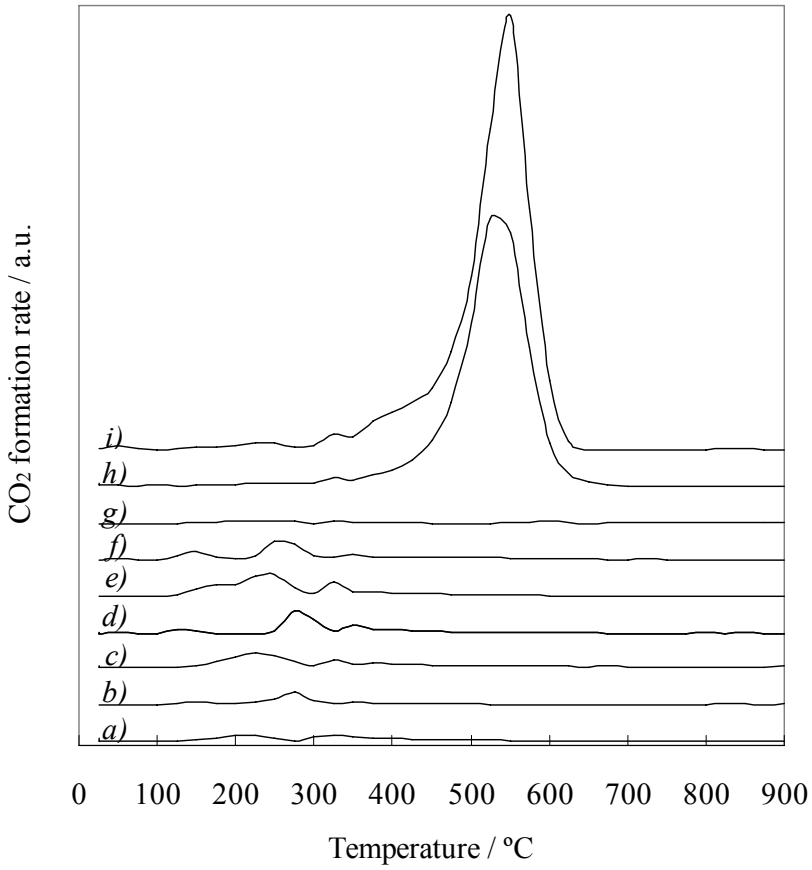

Figure 11. K. Takehira et al.

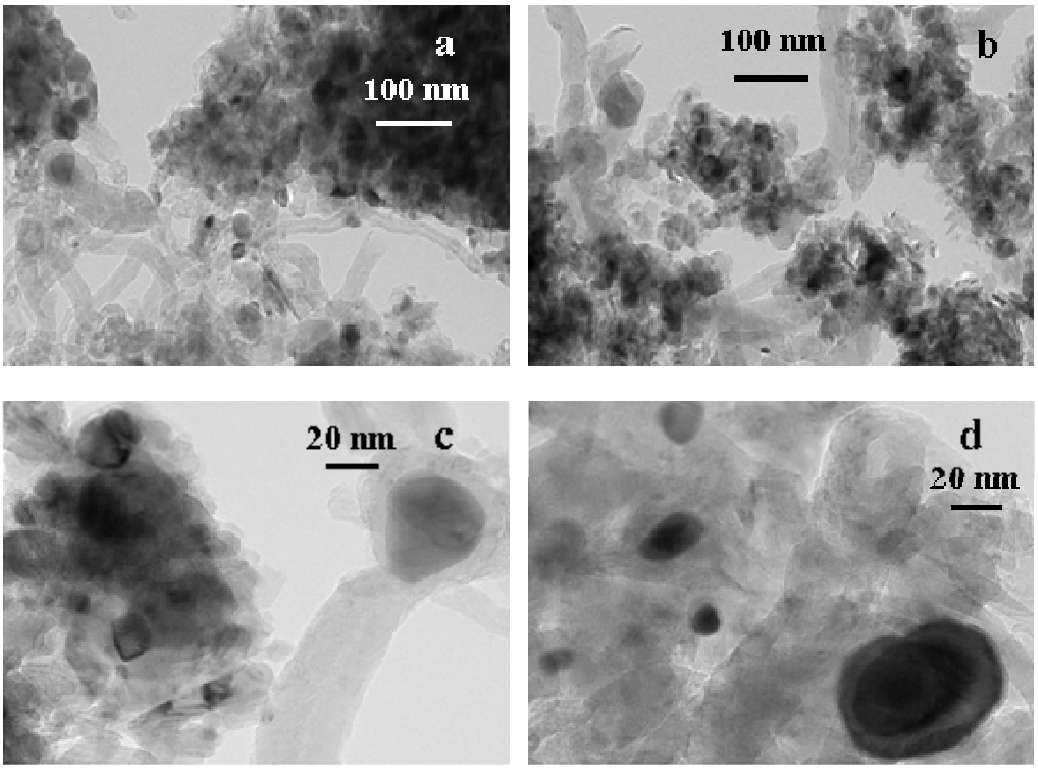

Figure 12. K. Takehira et al.